JOURNAL OF Materials CHEMISTRY

Carbon formed by hydrothermal treatment of α-SiC crystals

Thorsten Kraft* and Klaus G. Nickel

Institut für Mineralogie, Petrologie und Geochemie, Universität Tübingen, Wilhelmstraße 56, D-72074 Tübingen, Germany. E-mail: thorsten.kraft@uni-tuebingen.de

Received 6th October 1999, Accepted 10th December 1999

The hydrothermal behavior of α-SiC crystals has been studied in the temperature range 500–700 °C under 30–200 MPa pressure at different pH values. The extent of carbon formation *via* selective oxidative extraction of Si out of the SiC crystal lattice and the structure of the carbon formed depends on the experimental conditions. Homogeneous carbon coatings were obtained on machined crystal surfaces at *ca.* 600 °C and $p \geqslant 60$ MPa using distilled water. They were analysed using TEM, SEM, optical microscopy, micro-Raman spectroscopy, photoelectron spectroscopy, Auger spectroscopy and SIMS. The films consist of hydrogenated carbon which contains up to 13 atom% oxygen on the surface and *ca.* 3 atom% oxygen in the bulk. Predominantly amorphous sp^2-carbon formed, which shows little tendency to form turbostratic disordered or partly crystallized graphite. However, some particles containing nanocrystalline diamond were also found. A mechanism for hydrothermal carbon formation is proposed. The different methods for carbon analysis applied are compared.

1 Introduction

Carbon formation on SiC was first observed in the course of corrosion studies on tyranno (Si–Ti–C–O) fibers.[1,2] The investigations were extended to different SiC-materials[3] with a close look at β-SiC powders[4] and CVD-SiC fibers.[5]

Carbon coating on SiC is of interest for interface modification in ceramic composites and for the tailoring of tribological characteristics of SiC ceramics in valves, fittings and gaskets. In order to gain further information on carbon formation on SiC we extended the investigations to α-SiC crystals with well defined (0001) surfaces.

Thermodynamic calculation[5,6] revealed the possibility of carbon formation at water to SiC molar ratios $\leqslant 2$ in supercritical water *via* reaction (1)

$$SiC + 2H_2O = SiO_2 + C + 2H_2 \quad (1)$$

At water to SiC molar ratios > 2 complete dissolution should take place *via* reactions (2)–(4)

$$SiC + 2H_2O = SiO_2 + CH_4 \quad (2)$$

$$SiC + 3H_2O = SiO_2 + CO + 3H_2 \quad (3)$$

$$SiC + 4H_2O = SiO_2 + CO_2 + 4H_2 \quad (4)$$

However, at the surface of the solid SiC the water to SiC molar ratio has always been > 2 in experiments. Accordingly the carbon formation must have been primarily driven by the chemical kinetics of the reactions. These kinetics depend on the SiC materials used, as indicated by differences in extent, homogenity, and structure of the carbons formed on different SiC materials.

Carbon formation has been observed on any SiC material under investigation though it is restricted to small spots in some cases.[5] Homogeneous carbon coatings of graphitic hydrogenated carbon have only been obtained on tyranno fibers.[2] In this particular case, free carbon is present in the fibers, which can act as seeds for further carbon formation. In all other cases without intrinsically present free carbon the carbon formation is highly inhomogeneous.

In all these cases the structure of the carbon formed is of interest. Hydrothermal treatment of β-SiC powder yielded graphitic or amorphous sp^2-carbon as well as poorly crystallised diamond like sp^3-carbon.[4]

The potential for diamond synthesis *via* hydrothermal treatment of SiC was checked in a subsequent study.[7] Though formation of nanodiamond particles is evident, the final break-through concerning hydrothermal diamond synthesis is missing.

We concentrate on the formation and structure of carbon as revealed from the different analytical methods applied. The methods can be separated into:

(1) methods concerning the detection and structural characterisation of carbon (micro-Raman spectroscopy, TEM),

(2) methods concerning the observation of morphological changes (optical microscopy, SEM, FESEM), and

(3) methods concerning the composition of the carbon coating (AES, XPS/UPS, and SIMS).

Methods (1) and (2) covered the complete temperature–pressure range under investigation while the methods of type (3) were applied only to samples specially prepared at optimized conditions for carbon formation. However, only combination of all the methods can reveal conclusive and comprehensive information about the structure and the composition of the carbon formed.

2 Experimental

α-SiC crystals with sizes of $2 \times 2 \times 1$ or $4 \times 4 \times 1$ mm were cut out of SiC crystals formed as a side-product during the graphitisation of carbon by the Acheson process. If possible the as-grown (0001) faces of the SiC-crystals were left unmachined. About 70% of the (0001) faces of the crystals used were cut surfaces and grinding was necessary to obtain smooth surfaces with a roughness of < 1 μm. No free carbon was found on the crystals. They were thoroughly cleaned with water and propan-2-ol in an ultrasonic bath prior to use.

Three or four small crystals with 16 or 20 μl liquid,

respectively, were placed in gold capsules of 25 mm length and 3 mm diameter. Alternatively four large crystals and 30 μl liquid were enclosed in a gold capsules of 5 mm diameter and 25 mm length. Large crystals were processed only for subsequent analytical investigations which require larger surface areas. The liquids used were distilled water, and aqueous solutions containing 5 or 20% NaOH, 20% Na_2CO_3, 5% $NaHCO_3$, 20, 50 or 100% formic acid (HCOOH), and oxalic acid ($HOOC–COOH·2H_2O$). The capsules were sealed by welding. The experiments were conducted in tube-type cold-seal high-pressure vessels made of René 41 alloy. Most of the experiments were conducted in an horizontal arrangement under pressurization with water. Some experiments were conducted in an vertical arrangement under pressurization with argon. No differences in the results between both setups were observed.

After the experiments, the crystals and the walls of the gold capsules were examined using optical microscopy and micro-Raman spectroscopy. Two or more crystals of all samples, which show formation of carbon or formation of scales of silica, were treated with hot concentrated hydrofluoric acid for 30 min to remove the silica. Attempts to remove the silica scales by ultrasonic treatment in water failed.

3 Analytical methods

Micro-Raman spectroscopy is the most simple and powerful tool for analyzing and identifying more or less all different forms and allotropes of carbon and carbonaceous materials.[8] In this study it allowed for the detection and analysis of small spots (<1 μm^2) of free carbon and very thin carbon films of *ca.* 10 nm thickness. A Dilor Labram I micro-Raman spectrometer equipped with a He–Ne laser working at 632.8 nm was used to record the spectra. The spectrometer allowed for a spatial resolution of 1 μm using a $\times 100$ objective lens and a spectral resolution of 2 cm^{-1}.

The morphology and microstructure of crystal surfaces and carbon coatings were examined by optical microscopy, scanning electron microscopy (SEM) and field emission SEM (FESEM).

The carbon nanostructure was investigated by transmission electron microscopy (TEM) using a JEOL 3010 300 kV instrument. Particles and flakes liberated in the course of the HF-leaching procedure of the crystals after hydrothermal treatment were immersed in water by ultrasonic treatment and collected on 200 mesh copper grids covered with Lacey carbon film with large holes.

Photoelectron spectra (PS) were recorded using nonmonochromatized Mg-Kα radiation of 1253.6 eV for the XPS core-level spectra and a helium discharge lamp emitting at 21.22 eV (He I) and 40.82 eV (He II) for the UPS valence shell spectra. Four large SiC crystals were arranged on the sample holder to give a square of 8×8 mm to cover the beam area.

Survey scans were recorded to check for the elements present and for calibration of the energy scale. Special attention was given to the regions of kinetic electron energies of 690–735, 930–985 and 1075–1115 eV, which correspond to the binding energies of the electrons in the levels O $1s_{1/2}$ (532 eV), C $1s_{1/2}$ (284 eV) and Si $2s_{1/2}$ (149 eV), respectively in the XPS spectra. These regions were recorded with repeated scans and reduced stepwidth to obtain optimized signal to noise ratios of the peaks. After background and satellite subtraction the integral intensity of the peaks was obtained by fitting with mixed Gaussian–Lorentz functions. The intensities were corrected for the sensitivity of the transitions and related to each other in order to obtain an estimate of the C, O and Si contents on the surface. This method does not allow for a good quantitative determination of these elements but is sensitive to changes in the composition. In the UPS spectra only the He II region with binding energies up to 20 eV was recorded at good quality. The spectra were fitted using exponential background correction and Gaussian curves. After taking the first set of spectra the sample was sputtered with Ar^+ accelerated by 10 kV at a total current of *ca.* 2 μA. Further spectra were recorded after accumulated sputtering times of 15 min (XPS and UPS), 1 h (XPS) and 2 h (XPS).

Auger spectra were recorded under continuous Ar^+ sputtering to avoid extensive charging of the sample. The scans covered the electron kinetic energy range between 50 and 600 eV and allowed for the observation of the KLL lines of C and O and the LMM lines of Si and Ar.

Secondary ion mass spectroscopy (SIMS) was used to record depth profiles of specific elements at their atomic masses. Additional complete mass spectra were recorded at the beginning and at the end of the mass scans for depth profiling. Positively and negatively charged secondary ions were recorded in separate experiments under continuous sputtering with Ar^+ ions accelerated by 10 kV with following parameters:

1. Positively charged secondary ions.
   (a) Mass spectrum before depth profiling: 1.1 nA ion current on 0.7 mm^2.
   (b) Mass scans for depth profiling: 30 nA on 0.16 mm^2.
   (c) Mass spectrum after 1514 mass scans for depth profiling: 0.8 nA on 0.1 mm^2.
2. Negatively charged secondary ions.
   (a) Mass spectrum before depth profiling: 0.5 nA ion current on 0.7 mm^2.
   (b) Mass scans for depth profiling: 30 nA on 0.16 mm^2.
   (c) Mass spectrum after 1223 scans for depth profiling: 1 nA on 0.1 mm^2.

The PE, Auger and SIMS spectra were taken from ground surfaces of large SiC crystals HF-leached after 4 h processing at 600 °C and 200 MPa.

4 Results

4.1 Experiments with pure water

Optical microscopy shows changes especially on ground SiC surfaces. Some blackening of the ground matt silvery grey pristine surfaces was observed after 64 h at 500 °C and 200 MPa. No free carbon was detected by other analytical means in experiments performed at 500 °C.

Increase of the reaction temperature to 575–650 °C at 30–200 MPa in 4 h experiments yielded completely blackened surfaces. Additionally, black balls of micron size appeared after the experiments at 30 and 40 MPa.

At 650 °C also some loosly attached carbon deposits form while above 650 °C thick carbon layers of low adherence form. Macroscopic parts of the black coating are easily wiped off or delaminate upon HF-etching. After HF-etching uncoated parts appear, which look like the pristine surface. Fig. 1 shows black coated and silvery uncoated parts left after HF-etching of an SiC-crystal processed hydrothermally for 4 h at 700 °C and 200 MPa.

No change was observed on as-grown SiC surfaces processed at temperatures below 600 °C. Coatings were only found under conditions of strong carbon precipitation out of the fluid at 650 and 700 °C.

Deposits in the gold capsules formed at all reaction temperatures. At $T \leqslant 600$ °C white crystalline deposits form. At $T \geqslant 600$ °C the surface of the capsule becomes darker with increasing reaction temperature. Transparent films form up to 650 °C. Opaque black films and deposits form at 700 °C and sometimes at 650 °C. All dark films and coatings on the gold capsules could be wiped away easily.

Micro-Raman spectroscopy was applied to all samples. Carbon formation was detected after all experiments con-

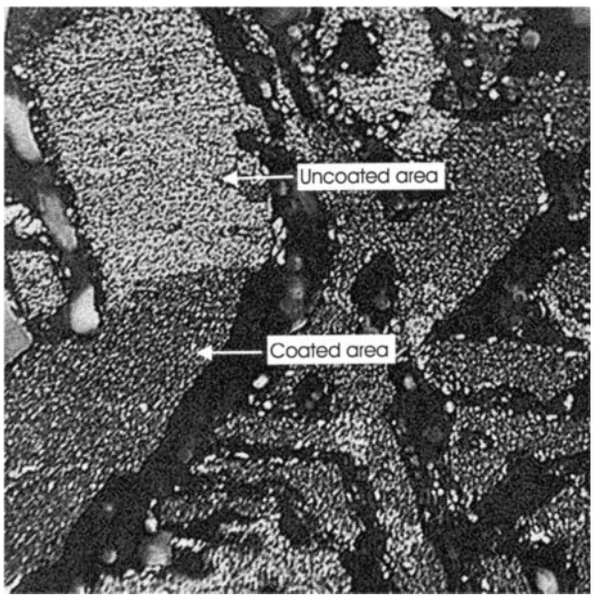

Fig. 1 Optical micrograph (area $1 \times 1\ mm^2$) of an α-SiC crystal treated for 4 h at 700 °C and 200 MPa with H_2O, HF leached.

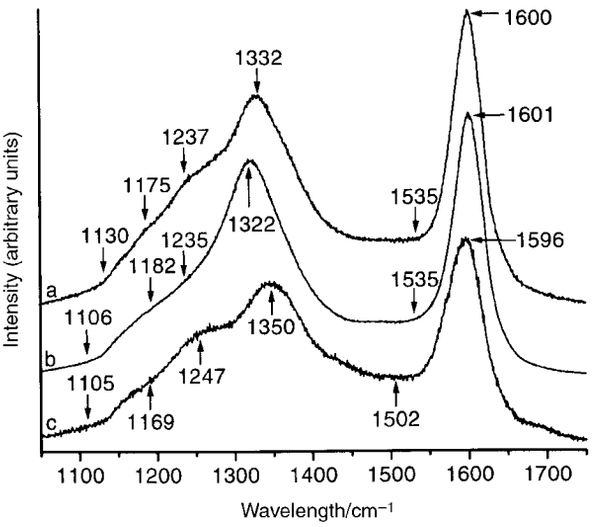

Fig. 2 Raman spectra of (a) a carbon film obtained on an α-SiC crystal treated for 4 h at 650 °C and 200 MPa with H_2O, HF leached, (b) a carbon deposit obtained after treatment of α-SiC crystals for 4 h at 650 °C and 200 MPa with H_2O and (c) anthracite; excitation at 632.8 nm.

ducted at and above 550 °C but only ground SiC-surfaces were uniformely coated.

The extent of the carbon formation increases with the reaction temperature and can be estimated from the intensity of the carbon bands and from the extend of coverage of the crystal surfaces. After experiments at 550 and 575 °C the surfaces are only partially coated. Carbon is primarily found in and at all grinding traces. Experiments at 600–650 °C yielded surfaces with complete and uniform carbon coating which remain after HF-etching. In contrast large areas without carbon coating are observed after HF-etching of samples processed at 700 °C.

No pressure dependence of the carbon formation was observed. However, after experiments below 50 MPa at 600 and 625 °C the coverage of the SiC surfaces was slightly incomplete.

No carbon growth was observed on as-grown surfaces. Carbon coatings appeared only under conditions of strong carbon precipitation out of the fluid at 650 and 700 °C and never appeared to be uniform.

The dark and black films formed in the gold capsules in experiments at and above 600 °C consist of carbon of the same type as the carbon films on the corresponding SiC crystals.

The white crystalline deposits formed in the gold capsules at experiments at and below 600 °C predominantly consist of partially hydrated SiO_2. Raman spectra showed the bands typical for quartz, cristobalite and water. The same kind of crystals were found on the SiC crystals prior to HF-etching. With the exception of keatite the products resemble the products found in the hydrothermal degradation study of CVD SiC fibres.[5] However, keatite formation can not be ruled out because its detection by Raman spectroscopy is difficult.

Depending on the reaction temperature, two slightly different typical Raman spectra of carbon were obtained [Fig. 2(a) and (b)]. They are very similar to the spectrum of anthracite [Fig. 2(c)].

Anthracite is a naturally occurring hard coal which shows some degree of graphitisation and low content of impurities when compared to other hard coals. However, it still contains considerable amounts of H, N and O from its organic precursers.

Spectrum (a) originates from carbon films and black balls and is observed after experiments performed between 550 and 650 °C on as-recovered SiC surfaces, on HF-etched SiC surfaces, and on gold capsules. Only the structure of the Raman bands in the region between 1100 and 1450 cm^{-1} appeared to be a little sharpened after HF-etching. Spectrum (b) originates from carbon deposits found on SiC crystals and in gold capsules after experiments at 700 and 650 °C.

The spectra were fitted with six independent mixed-Gaussian–Lorentz curves after linear background subtraction. Average values of fits of different similar looking spectra with estimated standard deviations are listed in Table 1. The fit data comprise the Raman shift and the normalized integrated intensity (% of the total intensity).

Some of the fitting curves can be assigned to vibrational bands known from graphite and amorphous carbons. The curves at *ca.* 1600 cm^{-1} can be attributed to a mixture of the graphite G-band, which is the only band present in single crystalline graphite at 1582 cm^{-1}, and the defect D′-band, present at disordered graphites at 1610 cm^{-1}.

The broad and large curve at *ca.* 1340 cm^{-1} represents the defect D-band which is absent in single crystalline graphite, but

Table 1 Averaged curve fit values of Raman shifts and relative band intensities for carbon films, carbon deposits and anthracite corresponding to Fig. 2

	Raman shift/cm^{-1}				Intensity (%)			
Band	C-film	C-deposit	Anthracite	Deviation	C-film	C-deposit	Anthracite	Deviation
G+D′	1601	1601	1596	2	17.1	16.5	16.7	1.2
A	1534	1531	1502	3	20.7	20.1	29.1	2.5
D	1339	1326	1350	6	46.4	53.5	29.0	3.2
pre 1	1242	1239	1247	6	9.8	2.6	21.3	2.7
pre 2	1177	1182	1169	9	3.7	5.5	1.8	1.5
pre 3	1122	1100	1105	12	2.3	1.6	2.2	0.9

becomes active in microcrystalline graphite owing to size effects. Its intensity increases with decreasing particle size and becomes prominent in nanosized graphite and amorphous sp^2-carbons. The average lateral size of the graphitic units was estimated from the intensity ratio of the G- and D-band of graphite.[9]

Broad curves at *ca.* 1530 cm^{-1} are necessary in most instances for a good fit of Raman spectra of carbon blacks[10] and are typical for amorphous carbons. In amorphous diamond-like carbon this band is conventionally attributed to sp^2-bonded carbon clusters in the sp^3-network.[11] There are no special assignments for the curves at *ca.* 1240, 1180 and 1110 cm^{-1} and these are denoted prebands 1, 2 and 3, respectively. Their origin is uncertain, but they are commonly observed in nanocrystalline diamond films.[12]

The significant difference between the spectra of the carbon films and the carbon deposits is the slope in front of the D-band which shows two bulges for the former but only one bulge for the latter. Fitting shows significant differences regarding the D-, pre 1- and pre 2-bands. Most notably, the intensity of the pre 1-band, responsible for the extra bulge in the spectrum of the carbon films is diminished in the spectrum of the C-deposit, while the D-band is downshifted from *ca.* 1339 cm^{-1} to *ca.* 1326 cm^{-1}. Less distinctive but of note is the intensity gain of the D- and pre 2-band.

The spectrum of anthracite is somewhat similar to the spectrum of the carbon film. However, the fit reveals pronounced differences to both the carbon film and the carbon deposit. The positions of the G + D′-, A- and D-bands are shifted and the intensity of the A- and pre 1-band is enhanced at the cost of the D-band.

Other kinds of carbon particles are also detected by Raman spectroscopy (Fig. 3) but the extent of their formation is always low. Particles of graphitic carbon of low structural order [Fig. 3(a)] were found predominantly after experiments conducted at temperatures up to 575 °C. At and above 650 °C some particles of graphitic carbon were evident [Fig. 3(b)]. Compared to the graphitic particles in Fig. 3(a), their structural order appears to be increased as indicated by the decrease of the width of the D-band and the splitting of the band at *ca.* 1600 cm^{-1} into a G-band component at 1581 cm^{-1} and a D′-band component at 1607 cm^{-1}.

Sometimes agglomerates of small colourless or transparent black crystals on SiC crystals or small light inclusions in carbon films, which exhibit a very narrow Raman band at *ca.* 1325–1330 cm^{-1}, were found after experiments conducted between 550 and 650 °C. This Raman band is typical for nanocrystalline diamond. Owing to size effects the band typical for diamond single crystals at 1332 cm^{-1} can be downshifted to *ca.* 1320 cm^{-1}.[13] The diamond particles and inclusions showed up randomly. Typically, the narrow band of nanocrystalline diamond appears in addition to the spectrum typical for carbon films in our spectra [Fig. 3(c)]. However, detection of small quantities of diamond in the presence of graphitic carbon is difficult using Raman spectroscopy with excitation in the visible range. The Raman scattering cross section of sp^3-carbon is low compared to sp^2-carbon but increases with decreasing wavelength[14] and becomes comparable in the UV range.[15]

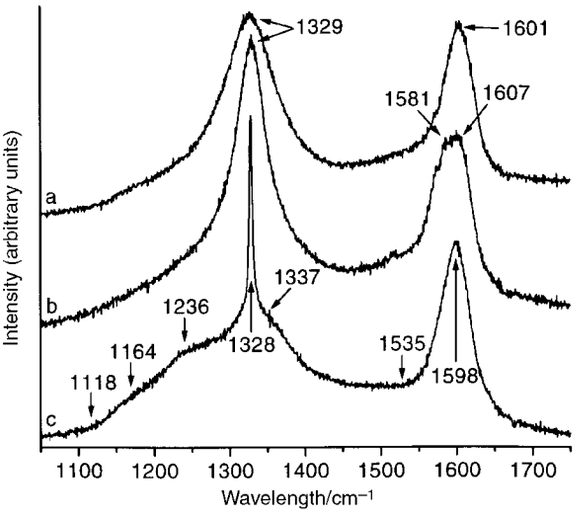

Fig. 3 Raman spectra of (a) a particle of graphitic carbon obtained after treatment of α-SiC crystals for 4 h at 575 °C and 50 MPa with H_2O, (b) a particle of graphitic carbon obtained after treatment of α-SiC crystals for 4 h at 650 °C and 200 MPa with H_2O and (c) of nanocrystalline diamond in a carbon film obtained on an α-SiC crystal treated for 4 h at 600 °C and 200 MPa with H_2O; excitation at 632.8 nm.

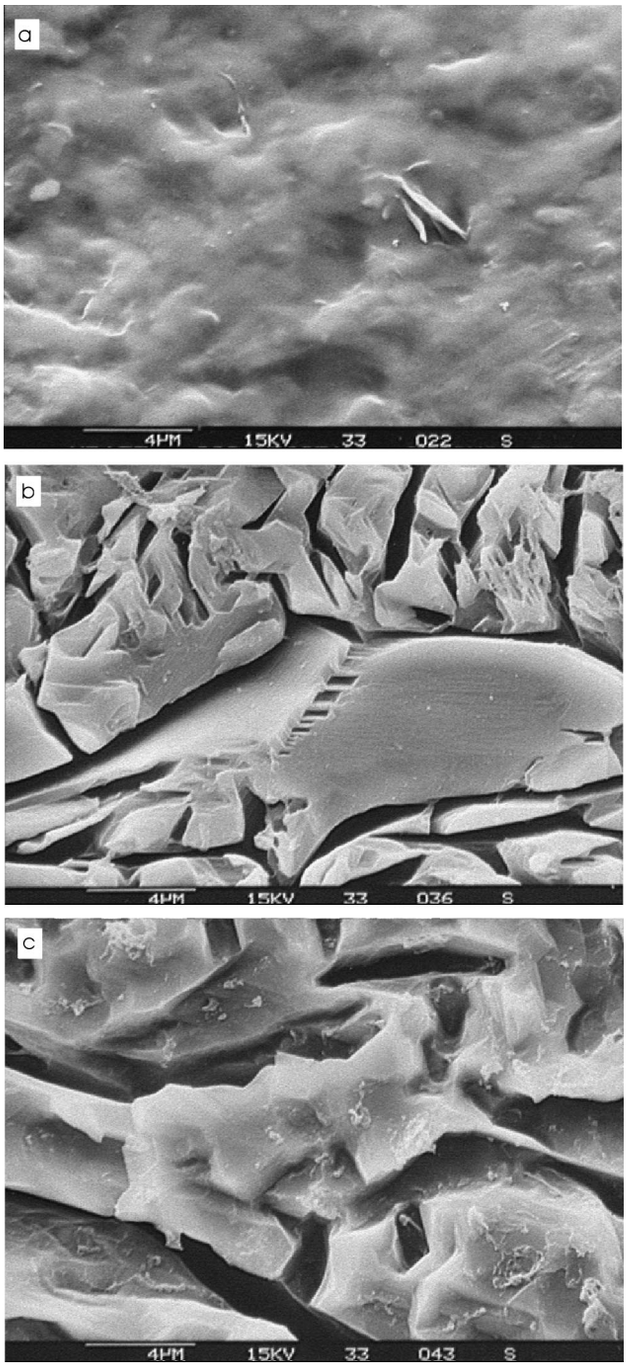

Fig. 4 SEM micrographs of ground surfaces of α-SiC crystals: (a) pristine, (b) after treatment with H_2O for 4 h at 600 °C and 200 MPa, HF leached, (c) after treatment with H_2O for 4 h at 700 °C and 200 MPa, HF leached.

Thus formation of diamond-like sp^3-carbon in the carbon films and deposits formed on the SiC crystals can not be ruled out using Raman spectroscopy with excitation at 632.8 nm.

SEM investigations showed a smooth but uneven surface of the pristine sample [Fig. 4(a)]. Deep grooves of up to 1 μm width and *ca.* 1 μm depth were found after hydrothermal treatment for 64 h at 500 °C and 200 MPa. The surface between the grooves remains level. The same result was obtained after 4 h at 600 °C [Fig. 4(b)]. Severe etching of the surface in between the grooves is observed after 4 h at 700 °C [Fig. 4(c)]. In this case, incomplete coatings remain on the surface after HF-etching, and are interpreted as partly delaminated carbon films.

Up to reaction temperatures of 650 °C, SEM did not reveal the presence of carbon particles or coatings. Thus, the carbon films formed up to 650 °C must have been too thin to be observed by SEM.

FESEM investigations showed rounded or flaky particles and residues on hydrothermally processed SiC crystals after experiments at and above temperatures of 550 °C [Fig. 5(a) and (b)]. The abundance of these particles, which might be attributed to carbon, increases with increasing reaction temperature and resulted in delaminated flakes at 700 °C [Fig. 5(c) and (d)].

TEM investigations were performed on material liberated by HF-etching after hydrothermal processing. Though only very little material is needed, sufficient material could only be collected after experiments performed at and above 600 °C. The amount of material liberated increased with increasing reaction temperature. In general only rounded and flaky carbon particles are found [Fig. 6(a)].

Possible dependences of the nanostructure of the carbon particles on temperature and pressure were investigated. At 600 °C only amorphous carbon particles [Fig. 6(b)] form under 200 MPa. At the same pressure, an increase of reaction temperature to 625–650 °C leads to the formation of particles containing turbostratic disordered graphite, as well as amorphous carbon [Fig. 6(c)]. Turbostratic disordered graphite is indicated by parallel lines with spacings of *ca.* 0.35 nm.

Reactions at a pressure of 30 and 40 MPa at a temperature of 600 °C also yielded carbon balls [Fig. 6(d)]. Holes in these [Fig. 6(e)] might stem from SiO_2 which was lost in the leaching process. We interpret the carbon balls as being derived from SiO_2–C–composites.

Extensive formation of turbostratic disordered graphite was observed in samples processed at 30 and 40 MPa. Thus, crystallization seems to be favoured with increasing temperature (as expected) and decreasing pressure (not expected). No diamond was found in this TEM study.

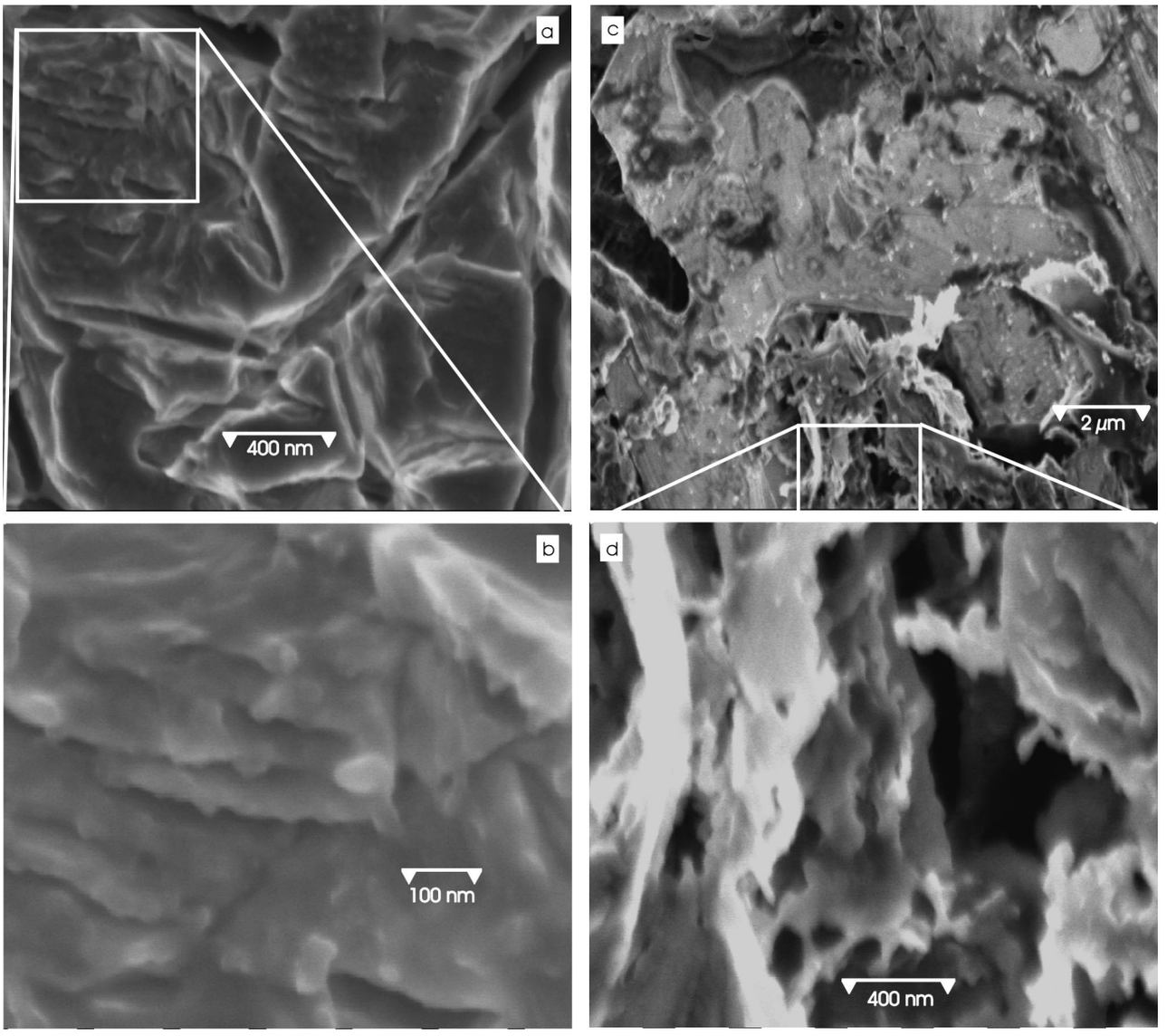

Fig. 5 FESEM micrographs of ground surfaces of α-SiC crystals, HF leached after treatment with H_2O for 4 h at 200 MPa and (a, b) 550 °C, (c, d) 700 °C.

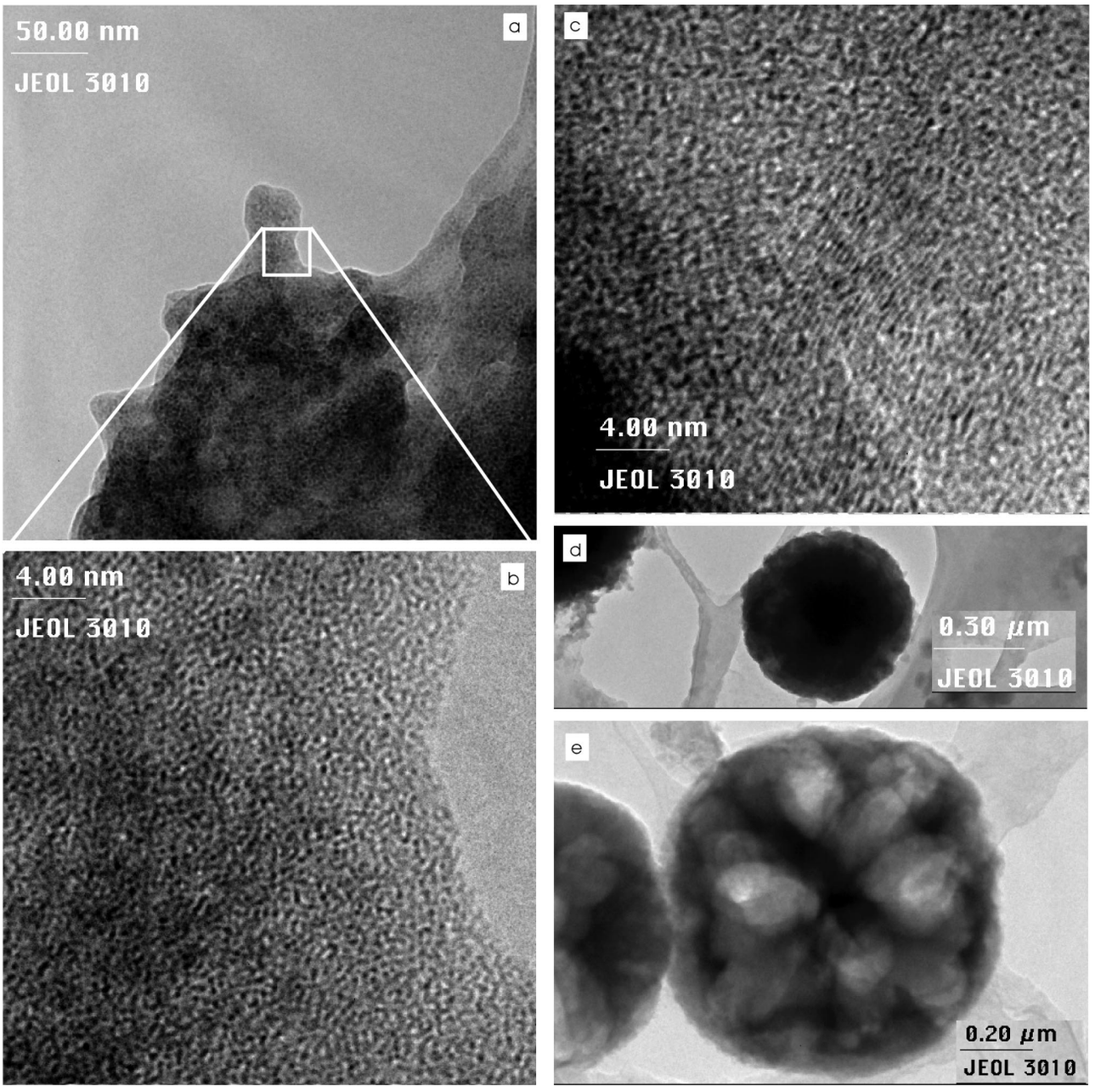

Fig. 6 TEM micrographs of (a, b) a flake of amorphous carbon from an α-SiC crystal treated for 4 h at 600 °C and 200 MPa with H_2O, HF leached, (c) amorphous carbon and turbostratic disordered graphite from an α-SiC crystal treated for 4 h at 650 °C and 200 MPa with H_2O, HF leached and (d, e) carbon balls from an α-SiC crystal treated for 4 h at 600 °C and 30 MPa with H_2O, HF leached.

Auger survey scans allowed for the detection of C, Si, Ar and O (Fig. 7). The shape of the KLL Auger line for carbon (insert in Fig. 7) with peaks at electron kinetic energies of *ca.* 277, 264 and 251 eV is typical for graphite and quite different from the profiles of sp^3-carbon in diamond or SiC.

While we did not succeed in obtaining complete depth profiles for C, Si and O in reasonable quality, the stepwise decrease of the carbon intensity and some continuous increase of the oxygen intensity with sputtering time were evident.

XPS investigations were used to estimate the relative concentrations of C, Si and O without and after sputtering for 15 min, 1 h or 2 h (Table 2). No other elements were detected.

The data revealed the strongest change in the first 15 min of sputtering. Most significantly the concentration of *ca.* 13 atom% oxygen on the unsputtered sample drops to *ca.* 3 atom% after 15 min sputtering and stays constant thereafter. The silicon concentration increases continuously with sputtering time while the carbon concentration decreases. The increase of the carbon content in the first 15 min of sputtering of the sample can be attributed to the disappearance of oxygen. A corresponding strong increase of the silicon signal indicates incorporated SiC.

The high oxygen concentration on the top surface of the carbon film is attributed to the formation of alcoholic (C–OH), carbonylic (C=O) and etheric (C–O–C) functions which act as endgroups at single carbon atoms or as connecting groups between two carbon atoms and bind to dangling bonds of carbon. Below this top surface the composition of the remaining carbon film is constant.

UPS spectra obtained before and after 15 min sputtering showed significant differences (Fig. 8). The Fermi energy could not be precisely determined and was estimated to a corrected electron kinetic energy of 36.5 ± 0.5 eV. Because of this uncertainty we retained electron kinetic energy in the energy scale. Fitting procedures revealed three peaks each with binding energies of *ca.* 6.4 (65% intensity), 9.5 (23%) and 13.3 eV (12%) for the unsputtered surface and 2.2 (10%), 7.4

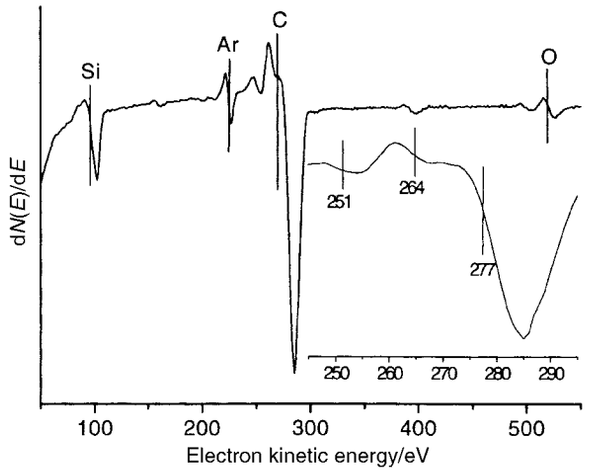

Fig. 7 AES spectrum of a surface of an α-SiC crystal treated for 4 h at 600 °C and 200 MPa with H_2O, HF leached.

(86%) and 13.8 eV (3%) for the sputtered surface. According to literature data[16–18] peaks at *ca.* 3, 6.5 and 13 eV correspond to binding energies of valence shell electrons in π and σ states in graphitic carbon and σ states in diamond, respectively. The spectrum of Fig. 8(b) closely resembles spectra of amorphous carbon, amorphous hydrogen containing carbon,[17] and sputtered graphite.[18] No spectrum corresponding to the spectrum of Fig. 8(a) has been found in the literature, which might be due to the high oxygen content on the surface of the hydrothermally formed carbon.

SIMS data gave some information about the surface species, the hydrogen content and the depth distribution of elements. Because of very different ionisation probabilities of the species and strong dependence of their ionisation probability on the hydrogen content, SIMS does not allow for quantitative analysis in this case but only for an estimation of the relative change of the concentration of the chemical elements. The advantage of SIMS is the possibility of easy detection of hydrogen and hydrogen containing species on our samples which is barely possible with the other methods.

The depth profile of selected negative ions (Fig. 9) shows a steep decrease of the H^-, O^- and C^- ion intensities within the time of the first five mass scans (Fig. 9, insert). This is followed by an asymptotic slope (which appears linear on a logarithmic scale) until the data become constant after *ca.* 300 mass scans. The ion yields in the mass scans 1, 5, 20 and 300 are listed and compared to each other in terms of ratios in Table 3. Compared to C^- and O^- the relative intensity loss at the beginning is pronounced for H^- and becomes close to the ratio for C^- with longer sputtering time. Compared to the C^- ratios, the O^- ratios are significantly higher only at the very first cycles and become significantly lower thereafter.

These data reveal that hydrogen is primarily situated on the outer surface of the carbon film. No sharp intensity changes were observed, as expected for coatings of uniform thickness.

Table 2 XPS determination of the relative atomic concentrations of O, C and Si as a function of the sputtering time on surfaces of α-SiC crystals HF leached after treatment for 4 h at 600 °C and 200 MPa with H_2O

	Atomic conc. (%)		
Sputtering time/min	O	C	Si
0	13.2	83.2	3.6
15	2.8	88.4	8.8
60	2.8	87.6	9.6
120	3.6	83.7	12.7

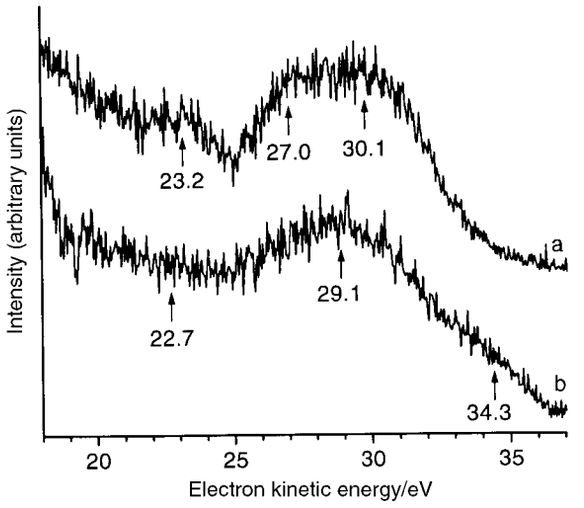

Fig. 8 UPS spectrum of a surface of an α-SiC crystal treated for 4 h at 600 °C and 200 MPa with H_2O, HF leached, (a) without sputtering and (b) after 15 min sputtering.

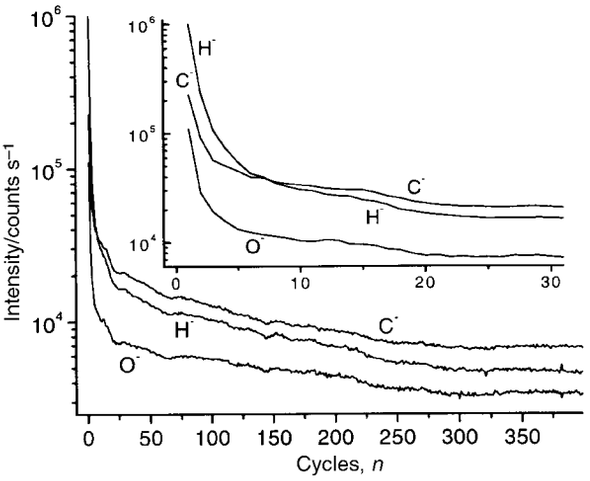

Fig. 9 SIMS depth profile scans for H^-, C^- and O^- of a surface of an α-SiC crystal treated for 4 h at 600 °C and 200 MPa with H_2O, HF leached.

In the depth profile for positive ions the ion yield at *m/z* 28^+ drops by *ca.* 35% in the time of the first five mass scans. Then, it asymptotically increases by *ca.* 132% until a constant value is reached after *ca.* 600 mass scans. According to the mass spectra in Fig. 10(c) and (d), the *m/z* 28^+ peak primarily originates from $C_2H_4^+$ in the first cycles before Si^+ becomes predominant. The increase of the *m/z* 28^+ peak is attributed to increasing areas of SiC.

Fig. 10 shows excerpts from mass spectra. The spectra from the beginning of the depth profile recordings [Fig. 10(a) and (c)] showed high yields of hydrogen and different hydrocarbon ions. Fragments such as $CH^{+/-}$, $CH_2^{+/-}$, CH_3^+, OH^-, $C_2H^{+/-}$, $C_2H_2^{+/-}$ and $C_2H_3^{+/-}$ in SIMS patterns of the surface suggest the existence of a large number of different organic endgroups. At the end of the depth profile recordings only the mass spectum of the negative ions [Fig. 10(b)] shows some remnants of hydrogen and hydrocarbon species. It is dominated by C_n^- ions.

The mass spectrum of the positive ions [Fig. 10(d)] is dominated by Si^{n+} ($n=1$–3) ions, which clearly show the isotopic distribution pattern of Si; C^+ and C_2^+ are also observed.

The mass spectra of the negative [Fig. 10(a) and (b)] and

Table 3 Ion yields and ratios for H^-, C^- and O^- of selected SIMS depth profile scanning cycles

	Element ion		
	H	C	O
Cycle 1 (I_1)	1,0003,850	225,937	110,258
Cycle 5 (I_5)	54,362	45,088	13,102
I_5/I_1	18.5	5.01	8.42
Cycle 20 (I_{20})	18,170	22,568	7,472
I_{20}/I_5	2.99	2	1.75
Cycle 300 (I_{300})	4,919	6,791	3,103
I_{300}/I_{20}	3.69	3.32	2.41

positive [Fig. 10(c) and (d)] ions showed high yields of O^-, OH^-, O_2^-, F^-, Cl^- and Na^+, Al^+, respectively. They appear in high yield because of high ionisation probabilities though they are present in low quantities.

4.2 Experiments using other fluids

Further experiments were performed with aqueous solutions containing 5 and 20% NaOH, 20% Na_2CO_3, 5% $NaHCO_3$, 50% sodium formate ($NaHCO_2$) and 20, 50, and 100 % formic acid (HCOOH), and oxalic acid ($HOOC–COOH·2H_2O$). Thus, a wide range of different pH values were studied.

Alkaline aqueous solutions of NaOH, Na_2CO_3, $NaHCO_3$ and $NaHCO_2$ were used at 200 MPa in the temperature range 500–650 °C. After the experiments the crystals were covered by colourless deposits which were removed by ultrasonic treament in cold water. No carbon formation was detected on the SiC crystals after any of these experiments.

Treatment with NaOH and Na_2CO_3 always resulted in strong etching, which leads to the formation of smooth shiny surfaces. Only water insoluble beads containing SiO_2 were found after treatment with Na_2CO_3 solution. Carbonate, detected by Raman spectroscopy after experiments with 5% NaOH solution, revealed intermediate formation of CO_2 from SiC. 5% $NaHCO_3$ solutions showed less SiC etching than for 5% NaOH with the surface only little affected and remaining rough.

Sodium formate was applied to act as an oxidation buffer stabilizing carbon formation according to reaction (1). Carbon formation upon hydrothermal decomposition can then proceed according to eqn. (5)

$$4NaHCO_2 + H_2O = Na_2CO_3 + 2NaHCO_3 + C + 2H_2 \quad (5)$$

However, no carbon formation was observed and the surfaces of the SiC crystals appeared the same as after treatment with NaOH and Na_2CO_3. XRD and Raman investigations revealed the formation of $Na_2CO_3·3NaHCO_3$ and Na_2CO_3 upon complete decomposition of $NaHCO_2$. Thus, the reactions of the hydrothermal decomposition are better described by eqns. (6) and (7)

$$4NaHCO_2 + 2H_2O = Na_2CO_3 + 2NaHCO_3 + CO + 3H_2 \quad (6)$$

$$4NaHCO_2 + 3H_2O = Na_2CO_3 + 2NaHCO_3 + CO_2 + 4H_2 \quad (7)$$

The experiments in acidic solutions were conducted at 600 °C and 200 MPa. No acids were present after the experiments. Both carbonic acids applied decomposed under the experimental conditions according to eqns. (8) and (9)

$$HCOOH = H_2O + CO \quad (8)$$

$$HOOC - COOH = H_2O + CO + CO_2 \quad (9)$$

No carbon formation was detected after these experiments. Application of 50% HCOOH or $HOOC–COOH·2H_2O$ yielded

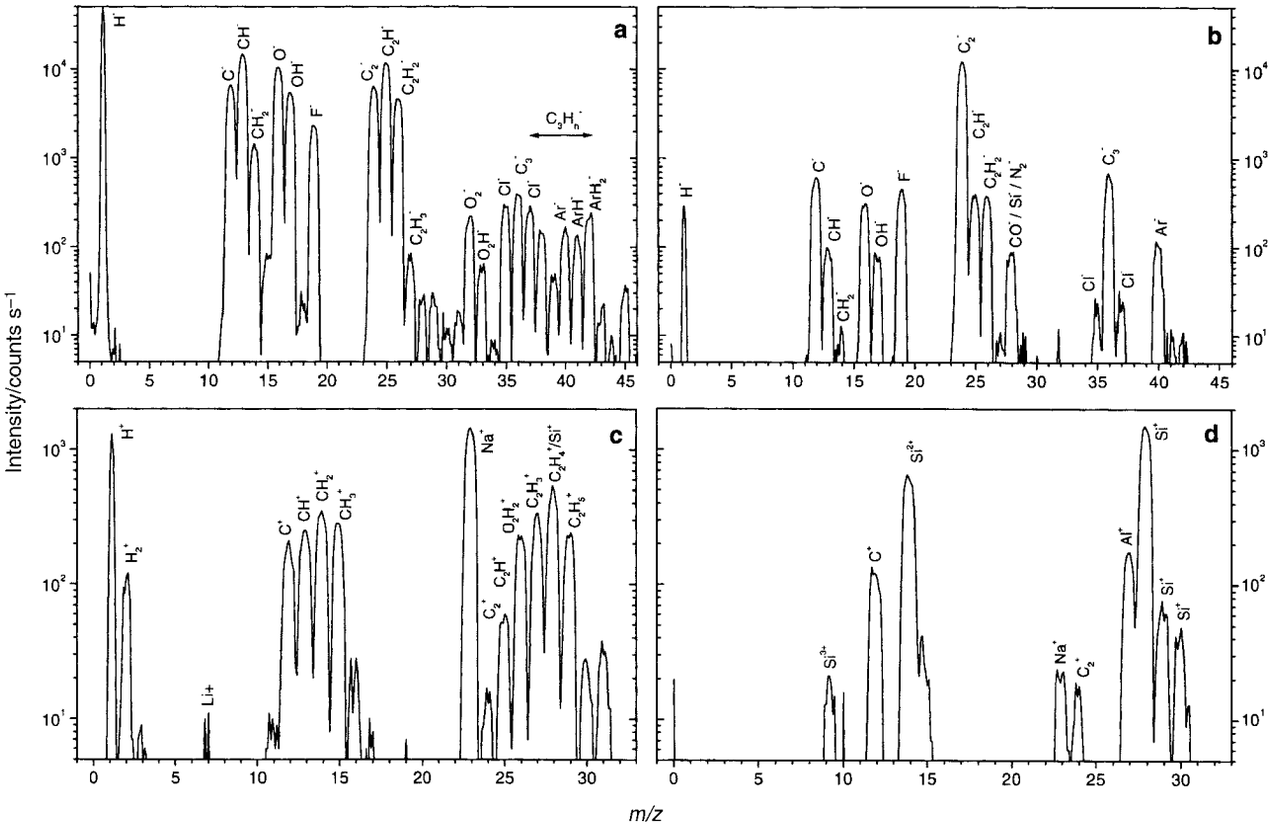

Fig. 10 SIM spectra of surfaces of α-SiC crystals treated for 4 h at 600 °C and 200 MPa with H_2O, HF leached, (a) negative ions before depth profile scanning, (b) negative ions after depth profile scanning, (c) positive ions before depth profile scanning and (d) positive ions after depth profile scanning.

a dense lawn of SiO_2 crystals on the SiC crystals. Only some SiO_2 crystals and a matted crystal surface appeared after the experiments with pure HCOOH and 20% HCOOH.

5 Discussion

Our investigations allow an evaluation of the hydrothermal behavior of α-SiC crystals, in the complete experimental range of 500–700 °C and 30–200 MPa.

As expected from thermodynamic calculations,[5] the effects due to changes in reaction temperature are much more pronounced than the effects due to change in pressure.

Carbon formation was only observed after experiments with pure water on ground SiC surfaces. All analytical methods showed increasing carbon formation with increasing reaction temperature.

The sensitivity for indication or detection of carbon is different for different techniques. Indication of carbon formation by optical microscopy, FESEM and SEM starts at reaction temperatures of 500, 550 and 650 °C, respectively. 550 °C was the lowest reaction temperature for carbon formation detection by Raman spectroscopy. Combination of optical microscopy, SEM and Raman spectroscopy showed that complete carbon coating with little corrosion and good reproducibility was achieved at 600 °C, 100–200 MPa and 4 h duration.

The carbon films obtained at $\leqslant$650 °C adhere well to the SiC crystals, while the carbon films on the gold capsules are easily wiped off. This indicates that most of the carbon on the SiC crystals forms directly from SiC by selective oxidative extraction of Si as exemplified by eqn. (1).

However, transport of carbonaceous species through the fluid to form carbon on surfaces also occurs. This is indicated by carbon films on the gold capsules after experiments conducted at and above 600 °C. The extent of this carbon deposition increases with increasing reaction temperature and becomes extensive at and above 650 °C.

The thickness of the carbon film on a given sample varies significantly, as revealed from depth profile scanning and micro-Raman data showing much carbon in grinding grooves but only a thin layer on the top of the SiC surface.

The carbon formed and its structure is best described as *amorphous sp^2-carbon* according to a combination of the TEM, Raman and AES results.

Investigations of its chemical composition by XPS, AES and SIMS showed considerable hydrogen and oxygen content, which differs considerably between the surface and the interior of the film. Hydrogen and oxygen are primarily bonded in organic groups located at the outer surface, saturating dangling bonds of carbon.

5.1 Mechanism of the carbon formation

Grinding of the SiC crystal surfaces appears to be crucial for homogeneous carbon formation. Comparable effects were observed in the course of CVD diamond synthesis on Si[19] and WC.[20] Enhanced diamond nucleation and growth were observed after polishing with a diamond paste. The reasons for these effects are not known. Direct nucleation on remaining diamond seeds appears to be unlikely because the surfaces were thoroughly cleaned after the grinding or diamond polishing treatment.

No hydrothermal carbon formation was observed from as-grown surfaces of the SiC crystals while a comparative study showed no carbon formation from SiC platelets. Hydrothermal treatment of different SiC powders including powdered α-SiC crystals at optimized reaction conditions revealed a low tendency for carbon formation.

We conclude that special surface states, which promote carbon nucleation, are crucial for carbon growth. They do not exist on as grown surfaces. They are only rarely present in crushed powders. They are best produced by grinding procedures.

From these observations we propose the following corrosion and etching mechanism:

(1) Based on the surface states the reaction starts with the formation of a very thin carbon film, which adheres closely to its underlying SiC support. This carbon film acts as a protective coating, thus slowing down the corrosion of SiC underneath.

(2) Presumably because of tension and/or gas formation, the carbon film cracks and allows for corrosion beneath these cracks. This corrosion leads to grooves, with the surface in between remaining untouched. Formation of grooves in the smooth surfaces was even observed after experiments at 500 °C, where no free carbon was detectable. This suggests that very thin carbon layers which are only a few monolayers thick possess reasonable protective properties.

(3) Increasing thickness of the carbon film promotes its delamination as observed especially after experiments at 700 °C. Then the top surfaces are also corroded. Delamination of the carbon film leaves an SiC-surface without surface states which leads to large areas without a carbon coating as exemplified in Fig. 1.

The use of alkaline or acidic fluids in the hydrothermal reactions instead of pure water proved to be deleterious for carbon formation and instead, increased corrosion was observed. We assume that the carbon seeding surface states are leached away too fast to allow for carbon nucleation in alkaline or acidic fluids.

5.2 Formation of diamond

Some particles and inclusions of nanocrystalline diamond were detected by Raman spectroscopy. Hydrothermal diamond synthesis is of great interest but attempts to increase the amount and/or size of the diamond crystals failed. The formation of only very small amounts of diamond in the presence of much more graphitic carbon is rationalized by heteroepitaxial formation of sp^2, sp^3 and mixed sp^2–sp^3 nuclei on ground SiC surfaces.

Formation of nuclei of sp^3-carbon might be extensive at an early stage of the hydrothermal reaction. Theoretical calculations suggest that nanometer sized diamonds should be thermodynamically more stable than nanometer sized graphite.[21] When the particles grow larger, graphite is thermodynamically more stable than diamond.

However, under hydrothermal conditions graphitic carbon is expected to grow faster than diamond. Promotion of diamond nucleation and growth would require selective destruction of graphitic carbon, suppression of graphite formation, and activation of the diamond surfaces. For example, in CVD diamond synthesis, graphitic carbon is selectively etched away by hydrogen atoms. Szymanski *et al.* claimed to have found hydrothermal fluids with these properties and reported the hydrothermal formation of diamonds of size 15–40 μm.[22] However, the composition of this fluid has not been disclosed. As yet, we were not able to establish such a selective etching procedure for the hydrothermal environment.

6 Summary

(1) Crystals of α-SiC were hydrothermally coated with amorphous sp^2-carbon through selective oxidative extraction of silicon. The best quality of the coating is obtained by treatment with pure water at 600–625 °C and 100–200 MPa for 4 h. No carbon coating was observed in caustic or acidic fluids. Formation of homogeneous carbon films was only observed on ground SiC surfaces.

(2) This procedure of carbon coating of α-SiC crystals is the second successful application of hydrothermal carbon forma-

tion out of SiC materials yielding homogeneous coatings. However, the formation of amorphous sp^2-carbon out of tyranno fibers[1,2] proceeds *via* nucleation on its content of free carbon which promotes the formation of thick and uniform carbon coatings on an amorphous SiC substrate. In our case scratching of the SiC surface promotes carbon formation and leads to very thin films on a crystalline SiC substrate.

(3) A mechanism, describing the hydrothermal carbon formation from SiC has been proposed.

(4) Diamond formation was detected, but yields and crystal sizes are very small.

Acknowledgements

We thank Mr J. Mällich, University of Tübingen (UT) for the manufacturing of the α-SiC-Crystals, Mrs M. Hertel (UT) for help with the experiments, Mr Hüttemann (UT) for help with SEM work, Mrs K. Jarosius, University of Illinois at Chicago (UIC) for help with FESEM work, Dr A. Nicholis (UIC) for TEM work, Prof. M. Trenary (UIC) for help with AES, Dr T. Weiss (UT) for help with UPS and XPS, and Mr M. Sinner (UT) for SIMS work. The study was supported by the DFG (grant Ni 299-4). Visits of T. K. at the UIC were made possible by a DAAD Fellowship. We are grateful to Prof. Y. Gogotsi and his coworkers and colleagues at the Department of Mechanical Engineering at the UIC for great hospitality and discussions.

References

1 Y. G. Gogotsi and M. Yoshimura, *J. Am. Ceram. Soc.*, 1995, **78**, 1439.
2 Y. G. Gogotsi and M. Yoshimura, *J. Mater. Sci. Lett.*, 1995, **14**, 755.
3 Y. G. Gogotsi and M. Yoshimura, *Nature*, 1994, **367**, 628.
4 Y. G. Gogotsi, K. G. Nickel, D. Bahloul-Hourlier, T. Merle-Mejean, G. E. Khomenko and K. P. Skjerlie, *J. Mater. Chem.*, 1996, **6**, 595.
5 T. Kraft, K. G. Nickel and Y. G. Gogotsi, *J. Mater. Sci.*, 1998, **33**, 4357.
6 N. S. Jacobson, Y. G. Gogotsi and M. Yoshimura, *J. Mater. Chem.*, 1995, **5**, 595.
7 Y. G. Gogotsi, P. Kofstad, M. Yoshimura and K. G. Nickel, *Diamond Relat. Mater.*, 1996, **5**, 151.
8 D. S. Knight and W. B. White, *J. Mater. Res.*, 1989, **4**, 385.
9 P. Lespade, R. Al-Jishi and M. S. Dresselhaus, *Carbon*, 1992, **20**, 427.
10 T. Jawhari, A. Roid and J. Casado, *Carbon*, 1995, **33**, 1561.
11 L. Y. Khriachtchev, R. Lappalainen, M. Hakovirta and M. Rasanen, *Diamond Relat. Mater.*, 1997, **6**, 694.
12 J. Wagner, C. Wild and P. Koidl, *Appl. Phys. Lett.*, 1991, **59**, 779.
13 Y. G. Gogotsi, T. Kraft, K. G. Nickel and M. E. Zvanut, *Diamond Relat. Mater.*, 1998, **7**, 1459.
14 M. Yoshikawa, *Mater. Sci. Forum*, 1989, **52**(53), 365.
15 K. W. R. Gilkes, H. S. Sands, D. N. Batchelder, W. I. Milne and J. Robertson, *J. Non-Cryst. Solids A*, 1998, **230**, 612.
16 P. Reinke and P. Oelhafen, *Diamond Relat. Mater.*, 1998, **7**, 175.
17 P. Reinke and P. Oelhafen, *J. Appl. Phys.*, 1997, **81**, 2396.
18 S. Schelz, T. Richmond, P. Kania, P. Oelhafen and H.-J. Güntherodt, *Surf. Sci.*, 1996, **359**, 227.
19 W. A. Yarbrough, *J. Am. Ceram. Soc.*, 1992, **75**, 3179.
20 R. Polini, G. Marcheselli and E. Traversa, *J. Am. Ceram. Soc.*, 1994, **77**, 2043.
21 P. Badziag, W. S. Verwoerd, W. P. Ellis and N. R. Greiner, *Nature*, 1990, **343**, 244.
22 A. M. Szymanski, E. Abgarowicz, A. Bakon, A. Niedbalska, R. Salacinski and J. Sentek, *Diamond Relat. Mater.*, 1995, **4**, 234.

Paper a908030i